5.6 kW peak power, nanosecond pulses at 274 nm from a frequency quadrupled Yb-doped fiber MOPA

JING HE,[*] DI LIN, LIN XU, MARTYNAS BERESNA, MICHALIS N. ZERVAS, SHAIF-UL ALAM, AND GILBERTO BRAMBILLA

Optoelectronics Research Centre, University of Southampton, Southampton, SO17 1BJ, United Kingdom
*J.He@soton.ac.uk

Abstract: A 2 W deep-ultraviolet (DUV) source at 274 nm with 5.6 kW peak power is demonstrated by frequency quadrupling a diode-seeded, polarization-maintaining (PM), Yb-doped fiber master oscillator power amplifier (MOPA) system delivering 1.8 ns pulses at a repetition rate of 200 kHz. The second harmonic generation (SHG) and the fourth harmonic generation (FHG) are achieved by using Lithium Triborate (LBO) crystal and $\beta-BaB_2O_4$ (BBO) crystal in sequence, with an IR-to-green and green-to-UV conversion efficiency of up to 65% and 26%, respectively. This is the first kW peak power pulsed UV system reported at 274 nm which has great potential for machining insulators, 2D materials, isotopic separation of Calcium-48, and fluorescence analysis of biological molecules.

OCIS codes: (140.7240) UV, EUV, and X-ray lasers; (140.3510) Lasers, fiber; (140.3615) Lasers, ytterbium; (190.2620) Harmonic generation and mixing; (140.4480) Optical amplifiers.

References and links

1. J. Zhang, K. Sugioka, and K. Midorikawa, "High-quality and high-efficiency machining of glass materials by laser-induced plasma-assisted ablation using conventional nanosecond UV, visible, and infrared lasers," Appl. Phys. A **69**, S879-S882 (1999).
2. O. M. Kirkby, M. Sala, G. Balerdi, R. de Nalda, L. Banares, S. Guerin, and H. H. Fielding, "Comparing the electronic relaxation dynamics of aniline and d(7)-aniline following excitation at 272-238 nm," Phys. Chem. Chem. Phys. **17**, 16270-16276 (2015).
3. C. Wagner, and N. Harned, "EUV lithography: Lithography gets extreme," Nat. Photonics **4**, 24-26 (2010).
4. Z. L. Li, H. Y. Zheng, G. C. Lim, P. L. Chu, and L. Li, "Study on UV laser machining quality of carbon fibre reinforced composites," Composites Part A **41**, 1403-1408 (2010).
5. L. Kolozsvári, A. Nógrádi, B. l. Hopp, and Z. Bor, "UV absorbance of the human cornea in the 240-to 400-nm range," Invest. Ophthalmol. Vis. Sci. **43**, 2165-2168 (2002).
6. J. Mes, E. J. van Duijn, R. Zinkstok, S. Witte, and W. Hogervorst, "Third-harmonic generation of a continuous-wave Ti:Sapphire laser in external resonant cavities," Appl. Phys. Lett. **82**, 4423-4425 (2003).
7. Q. Liu, and X. P. Yan, "High power all-solid-state fourth harmonic generation of 266 nm at the pulse repetition rate of 100 kHz," Laser Phys. Lett. **6**, 203-206 (2009).
8. D. A. V. Kliner, F. Di Teodoro, J. P. Koplow, S. W. Moore, and A. V. Smith, "Efficient second, third, fourth, and fifth harmonic generation of a Yb-doped fiber amplifier," Opt. Commun. **210**, 393-398 (2002).
9. R. Paschotta, J. Nilsson, A. C. Tropper, and D. C. Hanna, "Ytterbium-doped fiber amplifiers," IEEE J. Quantum Electron. **33**, 1049-1056 (1997).
10. X. Delen, L. Deyra, A. Benoit, M. Hanna, F. Balembois, B. Cocquelin, D. Sangla, F. Salin, J. Didierjean, and P. Georges, "Hybrid master oscillator power amplifier high-power narrow-linewidth nanosecond laser source at 257 nm," Opt. Lett. **38**, 995-997 (2013).
11. Q. Zeng, H. Liang, G. Zhang, M. D. Birowosuto, Z. Tian, H. Lin, Y. Fu, P. Dorenbos, and Q. Su, "Luminescence of Ce3+ activated fluoro-apatites M5(PO4)3F (M = Ca, Sr, Ba) under VUV–UV and x-ray excitation," J. Phys. Condens. Matter **18**, 9549-9560 (2006).
12. H. Guan, G. Liu, J. Wang, X. Dong, and W. Yu, "Multicolor tunable luminescence and paramagnetic properties of NaGdF(4):Tb(3)(+)/Sm(3)(+) multifunctional nanomaterials," Dalton trans. **43**, 10801-10808 (2014).
13. Y. Wei, H. Li, H. Hao, Y. Chen, C. Dong, and G. Wang, "β-Cyclodextrin functionalized Mn-doped ZnS quantum dots for the chiral sensing of tryptophan enantiomers," Polym. Chem. **6**, 591-598 (2015).
14. Y. Liu, C. Y. Liu, and Y. Liu, "Investigation on fluorescence quenching of dyes by graphite oxide and graphene," Appl. Surf. Sci. **257**, 5513-5518 (2011).

15. N. Kjaergaard, L. Hornekaer, A. M. Thommesen, Z. Videsen, and M. Drewsen, "Isotope selective loading of an ion trap using resonance-enhanced two-photon ionization," Appl. Phys. B **71**, 207-210 (2000).
16. K.-H. Ko, Y. Kim, H. Park, Y.-H. Cha, T.-S. Kim, L. Lee, G. Lim, J. Han, K.-H. Ko, and D.-Y. Jeong, "High-power continuous-wave tunable 544- and 272-nm beams based on a diode-oscillator fiber-amplifier for calcium spectroscopy," Appl. Phys. B **120**, 233-238 (2015).
17. H. Y. Chan, S.U. Alam, L. Xu, J. Bateman, D. J. Richardson, and D. P. Shepherd, "Compact, high-pulse-energy, high-power, picosecond master oscillator power amplifier," Opt. express **22**, 21938-21943 (2014).
18. G. D. Boyd, and D. A. Kleinman, "Parametric Interaction of Focused Gaussian Light Beams," J. Appl. Phys. **39**, 3597-3639 (1968).
19. A. Dubietis, G. Tamosauskas, A. Varanavicius, and G. Valiulis, "Two-photon absorbing properties of ultraviolet phase-matchable crystals at 264 and 211 nm," Appl. Opt. **39**, 2437-2440 (2000).
20. X. Mu, P. Steinvurzel, T. S. Rose, W. T. Lotshaw, S. M. Beck, and J. H. Clemmons, "High efficiency fourth-harmonic generation from nanosecond fiber master oscillator power amplifier," in *SPIE LASE*(SPIE, 2016), p.7.
21. H. Kouta, and Y. Kuwano, "Attaining 186-nm light generation in cooled beta-BaB2O4 crystal," Opt. Lett. **24**, 1230-1232 (1999).
22. M. Takahashi, G. Masada, I. Sekine, M. Cadatal, T. Shimizu, N. Sarukura, C. Byeon, V. Fedorov, S. Mirov, A. Dergachev, and P. F. Moulton, "Reduction of Nonlinear Absorption in Li2B4O7 by Temperature- and Repetition Rate-Control," Jpn. J. Appl. Phys. **48**, 11R (2009).

1. Introduction

Ultraviolet (UV) lasers are attractive solutions for many applications, such as machining [1], fluorescence research [2], and photolithography [3], because of their higher photon energy, smaller focus spots and larger absorption cross section in most materials in comparison to visible and infrared (IR) sources. In industrial applications, UV lasers are highly desirable for processing a wide variety of glasses, organics, semiconductors, carbon fiber reinforced plastics and ceramics [4]. It also plays an important role in medical treatment, e.g. ophthalmology, optical biopsy and laser microdissection [5].

High-brightness UV light is frequently obtained by nonlinear frequency conversion of Ti:Sapphire lasers with wavelength near λ~800 nm [6], and Nd-doped solid-state lasers [7] or Yb-doped fiber lasers [8] around λ~1 μm. Compared with bulk solid-state lasers, fiber lasers usually provide better beam quality, improved compactness, higher stability and efficiency. Besides, the Yb-doped fiber amplifier (YDFA) exhibits a relatively broad gain band in the near-IR wavelength range around λ~1-1.15 μm [9]. Therefore, MOPA systems can take full advantage of both the diode laser seed, which provides flexible wavelength tuning and serves as a frequency selector, and the fiber amplifier, which allows for the high brightness amplification over a wide wavelength range. It also enables similar advantages in the visible and ultraviolet when frequency conversion techniques are used. However, the maximum peak power extraction of a fiberized MOPA system is usually limited by the onset of nonlinear effects, such as self-phase modulation (SPM) and stimulated Raman scattering (SRS). Several techniques have been applied to reduce these effects, such as minimizing the total fiber length including both active and passive fibers, increasing the fiber core diameter while preserving the single-mode propagation, and limiting the pulse peak power.

Most of the reported UV sources produced through harmonic generation are peaked at around λ~257 nm and λ~266 nm [7, 10], correspond to the fourth harmonic of Yb or Nd-doped solid state lasers at gain peak of 1030 nm and 1064 nm, respectively. UV emissions at λ~270 nm has rarely been investigated, despite having many potential applications. For example, lanthanides such as Ce, Gd, have shown interesting energy transfer under excitation around λ~272-275 nm [11, 12]; many materials, such as tyrosine and graphene, have strong absorption when excited at λ~274 nm [13, 14]; important isotopes, like calcium-48, having a resonant wavelength around λ~272 nm corresponding to the $4s^2$ $^1S_0$–$4s5p$ $^1P_1$ transition [15].

Several lasers based on crystal or semiconductor materials have been reported to generate λ~272 nm continuous wave (CW) laser radiation by frequency quadrupling [6, 15, 16], with the highest reported power around 1 W; however, no high peak power pulsed UV radiation has been reported to-date. The difficulty originates from the fact that λ~1.1 μm emission is close to the edge of the Yb gain band. This necessitates a long active fiber to push the gain peak towards

the longer wavelength edge and as such the maximum peak power extraction is primarily limited by the nonlinear effects within the long device length.

Here we present a narrow-linewidth 2 W DUV source at λ~274 nm with high peak power up to 5.6 kW, by frequency quadrupling a fiberized, diode-seeded, PM YDFA MOPA system. The MOPA generated 1.8 ns pulses at λ~1097 nm with average output power of more than 13 W at a repetition rate of 200 kHz. High pulse peak power was achieved by gain partitioning in various amplification stages with fiber parameters appropriate to promote laser gain at λ~1.1 μm whilst minimizing nonlinear effects during the power scaling. The SHG and the FHG were achieved by using LBO crystal and BBO crystals in sequence, providing an IR-to-green and green-to-UV conversion efficiency as high as 65% and 26%, respectively.

2. Experimental setup

2.1 Yb-doped master oscillator power amplifier at λ~1097 nm

The schematic diagram of the PM YDFA MOPA system as well as the SHG and FHG stages is illustrated in Fig. 1. The seed laser was based on a linearly-polarized tunable Fabry-Perot laser diode (Sacher Lasertechnik). The center wavelength of the seed signal was set to λ~1097 nm by adjusting an internal diffraction grating with a linewidth of about 100 kHz. Optical output of the seed laser was pre-shaped into Gaussian-like pulses using a high extinction ratio (>30 dB) electro-optic modulator (EOM) driven by an arbitrary waveform generator (AWG). The pulse width of the EOM output was set to 2 ns at a repetition rate of 5 MHz.
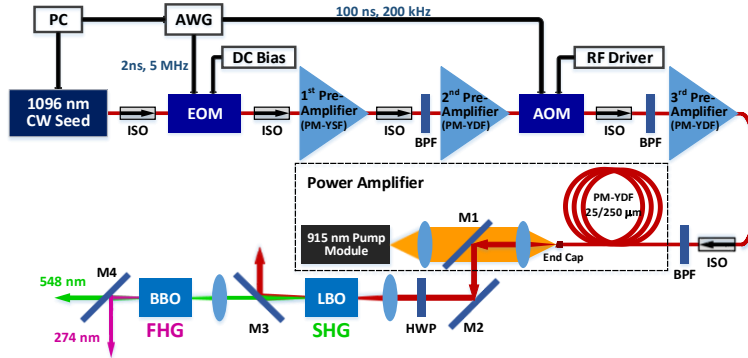

Fig. 1. Schematic diagram of the PM YDFA MOPA and the SHG and FHG system

An average seed signal power of 0.3 mW at the out of the EOM was amplified in a four-stage PM YDFA MOPA chain. The first preamplifier consisted of a 9 m long, core-pumped, PM Yb-doped fiber (YDF) with a core diameter of 5 μm and numerical aperture (NA) of 0.12. The type and length of active fiber was chosen to provide maximum amplifier gain towards λ~1100 nm. The amplifier was pumped in a co-propagating configuration by a 300 mW 976 nm single-mode laser diode and provided an average output power of 10 mW. The output of the first stage amplifier was coupled into the second preamplifier stage via an in-line PM isolator (ISO) and a PM band-pass filter (BPF). Similar arrangements were adopted across the amplifier chain to prevent spurious lasing to occur and suppress the build-up of short wavelength amplified spontaneous emission (ASE).

The active fiber of the second preamplifier was 10 m long, double-clad PM YDF (PLMA-YDF-10/125-HI-8, Nufern) with a core/cladding diameter of 11.5/125μm, and core/cladding NA of 0.08/0.46. The gain medium was pumped by a 915nm fiber-pigtailed broad-stripe diode laser through a fiberized pump combiner with maximum output power of 3 W. The output of second stage amplifier was passed through a fiber-pigtailed acousto-optic modulator (AOM) acting as an optical gate to remove excess ASE between the pulses and to reduce the repetition rate from 5 MHz to 200 kHz to enable pulse energy scaling with moderate average output powers in the subsequent amplifiers. Due to the AOM insertion loss and the pulse repetition

frequency reduced by a factor of 25, a maximum average power of 9 mW was available to seed the third preamplifier which used the same parameters as the second amplifier. The maximum average output power from the third preamplifier was 0.12 W.

The power amplifier stage comprised of an 18 m long, cladding-pumped PM YDF (PLMA-YDF-25/250-VIII, Nufern) with a core/cladding diameter of 25/250 μm, and core/cladding NA of 0.06/0.46. Once again, the length of the active fiber in this stage was optimized by balancing between the conflicting requirements of nonlinearity management and short wavelength ASE suppression. Although the 25 μm core supports several transverse modes around $\lambda \sim 1$ μm, a robust single mode operation was obtained by coiling the active fiber to a diameter of 75 mm to introduce additional bend-induced losses for higher order modes [17]. To avoid damage to the output facet, a 2 mm-long pure silica mode-expanding end-cap was spliced to the fiber output end and angle polished to 8 degree to prevent the backward-reflected power from coupling into the fiber core. A compact 915 nm multimode pump diode module was used to free-space end-pump the final amplifier.

2.2 The second harmonic generation and the fourth harmonic generation

The collimated $\lambda \sim 1097$ nm MOPA output was frequency doubled to $\lambda \sim 548$ nm by using an LBO crystal ($3 \times 3 \times 30$ mm^3, $\theta = 90°$, $\varphi = 0°$, EKSMA OPTICS). This crystal was chosen for SHG because of its excellent properties, such as high damage threshold, high nonlinear coefficient and broad transmission band. Furthermore, noncritical phase matching (NCPM) of LBO is featured with no walk-off angle that implies a nearly diffraction-limited output beam, ideal for further frequency conversion (e.g. FHG into the UV regime). Prior to the focusing lens, the linear polarization output of the YDF MOPA was rotated with the help of a half-wave plate (HWP) to align to the principal axis of the LBO crystal for maximizing conversion efficiency. Laser radiation was focused in the center of the crystal with a waist diameter of 90 μm corresponding to a Rayleigh range of 9 mm. The pump beam was intentionally focused smaller than the confocal parameter for improving the conversion efficiency [18]. The crystal was cut for NCPM at an operating wavelength of $\lambda \sim 1097$ nm with anti-reflection coatings on both end faces at the relevant wavelengths and was placed in an oven for temperature tuning. Type I ($o_Z^\omega + o_Z^\omega \rightarrow e_{xy}^{2\omega}$) NCPM was obtained at a constant temperature setting of 115 °C for maximum frequency conversion. The output from the LBO was passed through a dichroic mirror (DM) which rejects the unconverted $\lambda \sim 1097$ nm pump radiation.

The FHG process from $\lambda \sim 548$ nm to $\lambda \sim 274$ nm was achieved by using a BBO crystal ($5 \times 5 \times 6$ mm^3, $\theta = 45.7°$, $\varphi = 90°$, EKSMA OPTICS), which has one of the largest effective nonlinear coefficient in the UV band with a good damage threshold and provides on aggregate a better performance than other types of nonlinear frequency conversion crystals available (e.g. KBBF and CLBO [7]). At this wavelength, NCPM could not be obtained, so type I critical phase matching was employed. The walk-off associated with this process in BBO was about 85 mrad, resulting in an asymmetric output UV beam at $\lambda \sim 274$ nm.

3.   Results and discussion

The maximum average output power of YDFA MOPA reached 13.6 W at the launched pump power of 31 W [Fig. 2(a)], corresponding to a slope efficiency of 53%. No power roll-off was observed at the maximum power level. The inset of Fig. 2(a) illustrates the laser pulse duration measured by a high speed photodiode (DET01CFC, Thorlabs) and oscilloscope (WaveSurfer 44Xs, LeCroy) at the maximum operating power. The pulses were slightly compressed to 1.8 ns after four stages of amplification. Figure 2(b) shows the laser spectrum at different power level measured with an optical spectrum analyzer (OSA, Yokogawa AQ6370D) with 0.5 nm resolution, indicating a signal to amplified ASE ratio of nearly 30 dB. The laser wavelength was centered at $\lambda \sim 1097.08$ nm. No significant nonlinear distortion such as SPM was observed at a laser power of 12.8 W and the spectral bandwidth (measured at -20 dB level with 0.02 nm resolution) was maintained at 0.16 nm. Further power scaling was primarily limited by the

nonlinear distortion experienced by the amplified pulses as well as the transfer of energy to the SRS line. Nevertheless, a narrow-bandwidth pulse source of more than 30 kW peak power around λ~1.1 μm was obtained, high enough to allow efficient frequency conversion process.
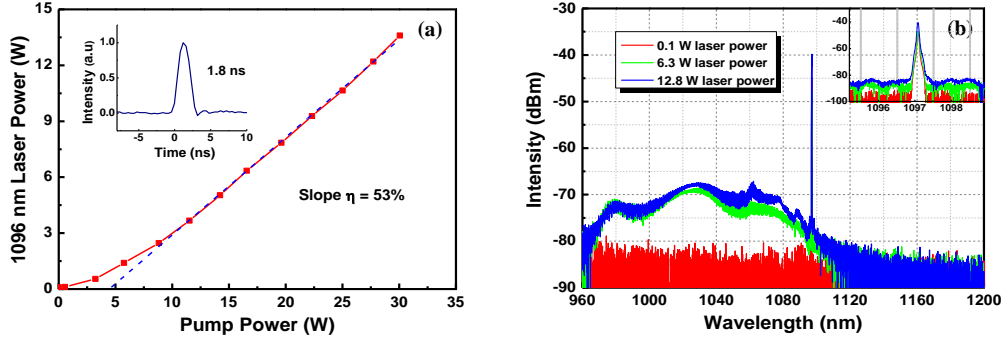

Fig. 2. (a) Output power from the power amplifier as a function of launched pump power (inset: Pulse duration measured at the maximum average output power of 13.6 W); (b) Spectra of the YDFA MOPA at different power levels (inset: detailed spectrum around λ~1097 nm)

Up to 8 W of SHG power at λ~548 nm was obtained at a fundamental power of 12.2 W corresponding to an overall optical conversion efficiency of 65% (Fig. 3). The measured polarization extinction ratio (PER) of 548 nm radiation was 30 dB under full power operation. The beam quality M^2 factor of the SHG signal based on D4σ method was measured to be 1.41 (x-axis) and 1.28 (y-axis) by using a scanning slit profiler (NS2s-Pyro/9/5, Ophir) at the SHG power of 6 W. The measured beam profile was shown in the inset of Fig. 3(b). It should be pointed out that the SHG power and the conversion efficiency could be higher since there was no roll-over observed. It is possible to improve the SHG power by further optimizing the focusing settings to achieve optimum generation conditions. However, it should be noted that there exists a trade-off between the power and the beam quality - more intense fundamental beam obtained through tight focusing into the LBO crystal may lead to degradation of the beam M^2 factor - which will have an adverse effect in the goal of achieving efficient FHG.
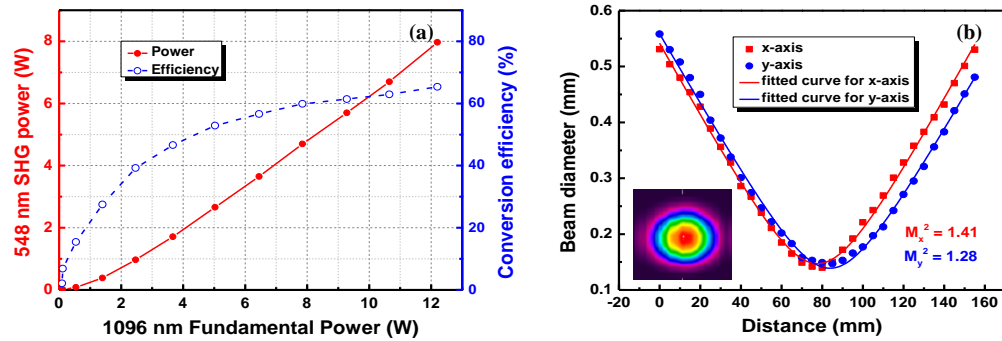

Fig. 3. (a) Average output power and conversion efficiency of the SHG signal at λ~548 nm as a function of λ~1097 nm fundamental power; (b) Measured beam quality M^2 at 6 W of SHG power (inset: Near-field beam profile)

A maximum output power of 2 W and peak power up to 5.6 kW (the pulse duration kept ~1.8 ns) at λ~274 nm was achieved when 7.6 W of green at λ~548 nm was launched into the BBO crystal [Fig. 4(a)], corresponding to a conversion efficiency of 26% from green to UV and 17% from IR to UV, respectively. The spectrum measured by a spectrometer (USB400, Ocean Optics) confirmed that the UV peak was centered at λ~274.2 nm [Fig. 4(b)]. As predicted, the ultraviolet output beam had an elliptical cross section (with beam quality M_x^2 ~ 1.52 and M_y^2 ~ 4.28) due to the spatial walk-off effect inside the crystal.

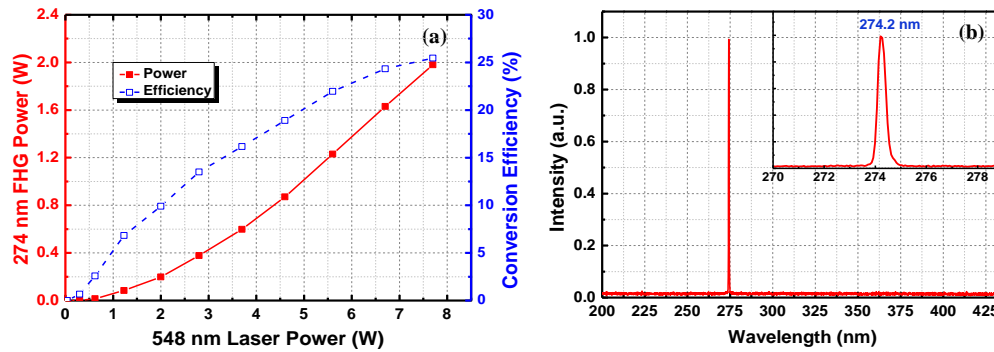Fig. 4. (a) Average output power and conversion efficiency of the λ~274 nm FHG vs. λ~548 nm power; (b) Spectrum of the λ~274 nm measured by the spectrometer (zoomed in the inset)

The limited conversion efficiency of the FHG could be due to several factors, including the limited peak power available of the λ~548 nm pump laser, the spatial walk-off due to the critical phase-matching condition of the BBO crystal and the imperfect M^2 values of the pump beam. Since there was no saturation of either UV power or conversion efficiency, tighter focusing aiming to improve the peak power density was investigated by changing the focusing condition. The diameter of the focused beam at the waist position was reduced from 60 μm to 30 μm for the green light. Instead of power increasing gradually as in Fig. 4(a), the generated UV experienced a much quicker growth at low incident green power, and reached 1.2 W at 3.9 W of λ~548 nm, corresponding to a conversion efficiency of 31%. However, the UV power quickly saturated and could not be increased even when the λ~548 nm power almost doubled; instead, the conversion efficiency dropped off quickly and the output power showed a downward trend. The reason for this is believed to be due to the strong two-photon absorption (TPA) [19] in the crystal as the tighter focusing caused the power density to reach GW/cm^2 level. Moreover, the TPA can be regarded as a heat source that locally increases the temperature and changes the refractive index, resulting in phase mismatching and a drop in output power [20]. Besides, the smaller beam size makes the walk-off play a dominating role in beam distortion, which also contributes further to the reduction in efficiency. On the contrary, under conditions of loose focusing and longer crystal lengths, efficiency may also drop due to the requirement of a narrower spectrum as the crystal acceptance bandwidth becomes smaller whilst the beam distortion gets worse due to larger aggregate walk-off distance in longer length of crystal. Possible solutions to balancing the output power and beam quality could be tighter thermal control of the harmonic crystal, such as the reduction of absorption coefficient in cooled BBO [21], and the repetition rate control of the incident pulses stream [22].

4. Summary

A 2 W UV laser at λ~274 nm with high peak power up to 5.6 kW was demonstrated by frequency quadrupling of a compact fiberized, diode-seeded, PM YDFA MOPA system operating at λ~1097 nm. The MOPA generated 1.8 ns pulses with average output power in excess of 13 W at a repetition frequency of 200 kHz. The IR-to-green (SHG) and green-to-UV (FHG) conversion efficiency were found to be 65% and 26% in LBO and BBO crystals, respectively. To our knowledge, this is the first high peak power pulsed UV system reported around λ~274 nm. This narrow-bandwidth source has great potential for applications in machining of insulators (clear glasses and plastics), 2D materials (e.g. graphene), isotopic separation of Calcium-48, and fluorescence analysis of biological molecules.

Funding